INTERNATIONAL JOURNAL FOR NUMERICAL METHODS IN FLUIDS
Int. J. Numer. Meth. Fluids **30**: 1091–1108 (1999)

FINITE ELEMENT SIMULATION OF STEADY STATE AND TRANSIENT FORCED CONVECTION IN SUPERFLUID HELIUM

L. BOTTURA[a,*] AND C. ROSSO[b]

[a] *CERN Division LHC-MTA, CH-1211 Geneva 23, Switzerland*
[b] *CryoSoft, 5 rue de la Belette, F-017 10 Thoiry, France*

SUMMARY

In this paper, the solution of transient mass, momentum and energy balances in superfluid helium are discussed by means of a finite element algorithm. A simple linearization procedure is used for the non-linear pseudo-diffusion term in the energy balance arising because of the unique counterflow heat transport mechanism in superfluid helium. The linearization algorithm is analyzed for accuracy order and stability. The reliability of the algorithm devised is shown in practical tests, comparing the numerical solutions with experimental data available in the literature. Copyright © 1999 John Wiley & Sons, Ltd.

KEY WORDS: finite element simulation; steady state; forced convection

1. INTRODUCTION

Helium is the only viable coolant for magnets built using low-temperature superconductors as it has the unique property of maintaining the liquid state till absolute zero [1]. The most common cooling modes range from *helium bath* (the superconducting magnet is completely submerged in a pool of helium at uniform temperature) to *natural convection* (buoyancy flow is used to establish a thermal syphon) to *forced flow helium* (the magnet is cooled by heat exchange to a forced flow of helium in cooling pipes). A common feature to all cooling modes is that magnets built using low temperature superconductors must be operated in a narrow range of temperatures, typically between 1.8 and 4.5 K. Further, independent of the nominal operating temperature level, they have in common the obvious necessity of having a well-known temperature distribution inside the magnet winding pack, so that the superconducting material can be operated with a safe margin with respect to the so-called *current sharing* temperature, where the superconductor starts to transit into the normal conducting state. Therefore, the prediction of the temperature profile inside a superconducting coil, taking into proper account the presence of the helium coolant, has deserved the attention in magnet design and testing, and in the development and validation of dedicated computer procedures (see for instance [2] and the references quoted therein).

Here we deal in particular with the solution of the mass, momentum and energy balances of helium when it is cooled below the *lambda* transition, a logarithmic anomaly in the specific heat, and achieves the so-called *superfluid* state. The boundary of the *lambda* transition is

* Correspondence to: CERN Division LHC-MTA, CH-1211 Geneva 23, Switzerland.

CCC 0271–2091/99/161091–18$17.50

Received September 1997
Revised July 1998

represented in the (p, T) helium state diagram by the pressure-dependent temperature $T_\lambda(p)$ called by analogy the *lambda* temperature. T_λ has been shown experimentally to be only weakly dependent on pressure, ranging from 1.77 K at the melting line (at 30 bar) to 2.17 K at the boiling line (at 50 mbar). Below T_λ, helium becomes a quantum fluid with vanishing apparent flow resistance through narrow capillaries and anomalously high heat transport capability [1]. Both properties are of interest for cooling applications because they imply high heat removal potential in conjunction with little pumping work at cryogenic temperature.

A good phenomenological description of these properties is given by the two-fluid model [1,3,4], which assumes that superfluid helium consists of two interpenetrating fluid components, a normal fluid and a superfluid. The inviscid superfluid component, with density ρ_s, has zero entropy, while the viscous normal component, with density ρ_n and viscosity v_n, carries the entropy of the mixture S. The two-fluid model states that the total density of the mixture ρ is given by the sum of the densities of the two coexisting species:

$$\rho = \rho_s + \rho_n, \tag{1}$$

and that the total momentum ρv is given by the sum of the momenta of the single species:

$$\rho v = \rho_s v_s + \rho_n v_n, \tag{2}$$

where v_s and v_n are the velocities of the superfluid and normal components respectively. The vanishing viscosity of the superfluid component explains why superfluid helium can flow with no impedance through porous media that would otherwise present a large impedance to a normal fluid.

The concentration of the two species depends on temperature. Above T_λ, the superfluid concentration is zero, but it increases as the temperature is lowered below T_λ, replacing gradually the normal component. As an example, at 0.8 K the normal fluid represents only approximately 0.1% of the total fluid. Local heating of stagnant superfluid helium with a heat flux $\dot{q}''$ causes a change in the relative concentrations of the superfluid and normal components. To maintain mass equilibrium and zero momentum, according to Equations (1) and (2), a net flow of the superconducting component 'towards' the heat source, and of the normal component 'away' from the heat source must be established. Because the superfluid component has zero entropy it does not transport heat. On the other hand, the motion of the normal fluid component is associated with heat flow, and the heat transported is given by:

$$\dot{q}'' = \rho S T v_n. \tag{3}$$

This peculiar heat transport mechanism resembles mass convection in a normal fluid, but remember that it is not associated with a net mass flow of the helium mixture. It is often referred to as *counterflow* heat exchange, and is responsible for the exceedingly high heat transport capability of superfluid stagnant helium. To highlight typical orders of magnitude, a temperature gradient of 0.1 K m^{-1} would result in a conduction heat flux of 2 mW m^{-2} in normal helium at 4.2 K (above T_λ), while the counterflow heat flux under the same temperature gradient would be 30 kW m^{-2} in superfluid helium at 1.8 K (below T_λ). Heat transfer in superfluid helium is hence largely dominated by counterflow heat exchange, in turn governed by the hydrodynamics of the motions of the normal and superfluid components.

The normal and superfluid components tend to interact differently depending on the difference of velocities. On the other hand, Equation (3) implies a relation between the heat flux and the magnitude of the internal flow. For this reason the distinction of different regimes of interaction between normal and superfluid components is based directly on the heat flux, rather than on the velocities. For small heat fluxes, associated with small velocites v_n and v_s,

the interaction between the two components is negligible. This regime is referred to as *laminar* internal convection and is typical of heat exchange in channels with small diameter, below 10 μm. Increasing the heat flux, the interaction between the two components causes the generation of internal turbulence, that gives rise to a drag between superfluid and normal fluid. This interaction, also known as the Gorter–Mellink mutual friction mechanism [5], is typical of heat transfer in large channels with diameter in excess of 100 μm. For most cooling applications in superconducting magnets technology, heat fluxes and channels are large enough to have their heat flow controlled by the mutual friction mechanism [6], that is therefore, the heat transfer regime of widest practical interest.

The motion of the two components forming the superfluid helium is governed by a modified form of the classical Navier–Stokes equations [3,4,7]. The modifications consist of terms originating from the mutual friction term, discussed above, and from the chemical potential in the presence of a difference of velocity between the two components. These terms appear in the momentum equations of each single component, and cause a strong coupling with the energy equation. Because of the relevance for magnet construction and design we will focus here on simulation of channels with diameters in the millimeter range, containing stagnant or forced flow superfluid helium. Under these conditions, the two fluids are in the turbulent transport regime and mutual friction dominates. In addition, we will consider cooling circuits with large length-to-diameter ratios, typically in excess of 1000, so that the problem can be considered one-dimensional. Within these limits, the two-fluid model can be drastically simplified. As presented by Kitamura *et al.* [7], the continuity and momentum balances of the mixture of the two-fluid components, normal and superfluid, in terms of total density and density averaged velocity, are the same as for a single component normal fluid. Taking further the momentum balance for the superfluid component and neglecting acceleration, viscosity and pressure gradient terms, it can be shown that the Gorter–Mellink mutual friction term in the momentum balance for the superfluid component gives origin to a strong non-linear pseudo-conduction term in the energy transport equation (see, for instance, Arp [4], Kitamura [7] or Van Sciver [1,6]). This term accounts physically for the heat transported by the counterflow mechanism described above, and it is customary to write the associated heat flux as follows:

$$\dot{q}''_{\mathrm{cf}} = -\left(F(T,p)\frac{\partial T}{\partial x}\right)^{1/\eta}, \tag{4}$$

where $\dot{q}''_{\mathrm{cf}}$ is the counterflow heat flux in the x-direction. The helium thermodynamic state is defined by its temperature T and pressure p. The exponent $1/\eta$ is empirically determined and generally is in the range of 1/3. Finally, the effective conductivity function $F(T,p)$ is a property that has been tabulated from experimental data. We have reported in Figure 1 typical values of $F(T,p)$ for different helium pressures. The units of F are consistent only for $\eta = 3$, and we will therefore use this choice throughout the paper. Above the *lambda* transition, the value of F is identically zero, indicating that the counterflow mechanism disappears in normal helium. Equation (4) shows the high degree of non-linearity of the additional heat transport term, both because of the temperature and pressure dependence of the effective conductivity function F, and because of the presence of the exponent $1/\eta$ in the dependence of $\dot{q}''_{\mathrm{cf}}$ on the temperature gradient.

The result of the simplification process described above is a *single fluid* approximation, where only the energy balance is modified to model the counterflow heat transport. Heat transport in superfluid helium within the frame of this *single fluid* approximation has been solved by several authors, either by approximate analytical methods [9,11] or numerically [12–14]. Most of the numerical work performed so far is based on the use of dedicated

procedures (e.g. Runge–Kutta integration for steady state [12,14], upwind or staggered mesh finite differences [12] and FFT methods [7] for transients). Only the model of [13] is based on the same finite element procedure for steady state and transient simulation. The governing equations, in conservation form, are discretized there with a Taylor–Galerkin finite element algorithm [15] equivalent to the Lax–Wendroff finite difference solver for the Euler equations of compressible flow [16]. The equations are solved explicitly in time and, therefore, the algorithm suffers from strong limitations on the time step and mesh size related to the stability condition on the Courant number. The counterflow term is finally treated as an additional flux in the energy balance, also evaluated explicitly from the results of the previous time step, and hence prone to produce unstable results.

Our objective in this paper is to overcome these limitations, solving the equations for compressible flow of superfluid helium implicitly, using the same algorithm for transient up to steady state conditions. We will use as a starting point the formulation and finite element algorithm developed in [2], well-adapted to the analysis of one-dimensional steady and transient compressible flow in cooling channels containing normal helium. In the next section we will present the approximate, single fluid model for compressible flow in superfluid helium, including the counterflow heat flux. Section 3 describes in detail the finite element algorithm. The effect of the additional counterflow term on stability and accuracy is studied in Section 4. We will finally use published experimental data in Section 5 to benchmark the model and the solution procedure.

2. MODEL

As we discussed in the previous section, we concentrate here on one-dimensional compressible flow of superfluid helium, in conditions where heat transfer is dominated by the Gorter–Mellink mutual friction. Within this approximation, the mass, momentum and energy transport in superfluid helium are the same balances as for transient viscous, compressible flow of a normal fluid, provided that a non-linear term, Equation (4), is added in the energy transport equation. This term models the effect of the *counterflow* heat transfer mechanism. The common approach to the solution of one-dimensional compressible flow in pipes is to write the mass, momentum and energy conservation in terms of the conserved variables (mass, momentum and energy density). In [2], we found that a more convenient description of the

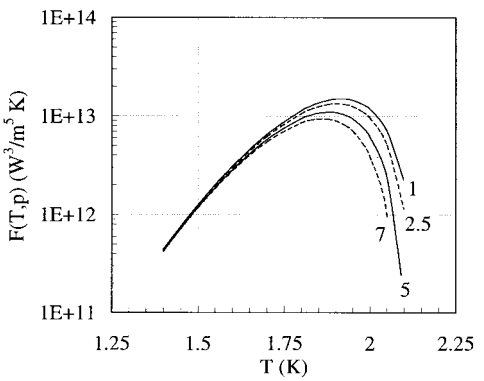

Figure 1. Superfluid heat conductivity function $F(T, p)$ at several pressures (indicated in bar on the curves). The function $F(T, p)$ is zero above the lambda temperature T_λ (in the range of 2.1 K).

one-dimensional transient flow can be obtained using velocity v, pressure p and temperature T as primary variables. We refer in particular to [2] for a complete derivation of the compressible flow equations for normal helium in these variables. In the case of superfluid helium, we need to add the counterflow heat transport term to the energy conservation balance. After trivial algebra, we can write the modified set of equations for a compressible, one-dimensional flow of superfluid helium:

$$\frac{\partial p}{\partial t}+\rho c^2\frac{\partial v}{\partial x}+v\frac{\partial p}{\partial x}=2f\rho\varphi\frac{v^2|v|}{D_h}+\varphi\dot{q}'''_{\mathrm{ext}}-\varphi\frac{\partial\dot{q}''_{\mathrm{cf}}}{\partial x}\qquad\text{continuity,}\tag{5}$$

$$\frac{\partial v}{\partial t}+v\frac{\partial v}{\partial x}+\frac{1}{\rho}\frac{\partial p}{\partial x}=-2f\rho\frac{v|v|}{D_h}\qquad\text{momentum,}\tag{6}$$

$$\frac{\partial T}{\partial t}+\varphi T\frac{\partial v}{\partial x}+v\frac{\partial T}{\partial x}=\frac{2f}{C_v}\frac{v^2|v|}{D_h}+\frac{\dot{q}'''_{\mathrm{ext}}}{\rho C_v}-\frac{1}{\rho C_v}\frac{\partial\dot{q}''_{\mathrm{cf}}}{\partial x}\qquad\text{energy,}\tag{7}$$

where the meaning of the symbols is mostly standard, and a complete list is reported in Appendix A. We stress that for a compressible fluid, the equations above are exact, i.e. they do not contain any thermodynamic approximation. In the case of superfluid helium, the set above is only a good practical representation of the more complex two-fluid physics [1,14]. We clearly see the advantage in the use of temperature as a state variable, namely the possibility of linearizing the counterflow heat transport term directly, as we will discuss in the next section. We have shown in [2] that the use of pressure as the second state variable allows us to achieve stable simulations at very large Courant number (in excess of 1000) with a simple linearization that does not involve iterative solution.

As noted by Arp [8], the thermophysical properties that appear in Equations (5)–(7) are either continuous (isentropic sound speed c, Gruneisen parameter φ) or weakly non-analytic (density ρ, specific heat at constant volume C_v) at the phase boundaries. This limits the error introduced in the vicinity of phase changes by uncertainties in the coefficients of the differential equations. In particular, the Gruneisen parameter φ, defined as:

$$\varphi=\frac{\rho}{T}\left(\frac{\partial T}{\partial\rho}\right)_S\tag{8}$$

(the derivative is taken at constant entropy S) is continuous and well-behaved, so that it is very useful in reducing the equations to a compact and well-conditioned form. The helium state equation $\rho(p,T)$ and the thermophysical properties are obtained from interpolations and fits of standard tables of measured points. The relative accuracy of these fits is of 1–3%, but can degrade by as much as one order of magnitude (10–30%) in close vicinity (less than 0.1 K) to the phase boundaries. The accuracy of the conductivity function F relative to its maximum is better than 10%. As we already mentioned, we take the exponent $1/\eta$ equal to 1/3 throughout this work. This is necessary to maintain consistency with the definition of F.

Under the assumption of large length-to-diameter ratios, the viscous force in the boundary layer is modeled as a *wall friction*, through a friction factor f that is related empirically to the Reynolds number of the flow. Several correlations can be found in the literature depending on the geometry of the flow channel and on the range of Reynolds number covered. We have chosen the following simple form that applies to a *smooth* tube:

$$
\begin{aligned}
f &= \max\{f_\mathrm{l}, f_\mathrm{t}\},\\
f_\mathrm{l} &= \frac{16}{Re},\\
f_\mathrm{t} &= \frac{0.046}{Re^{1/5}},
\end{aligned}
\tag{9}
$$

where the transition from laminar (f_l) to turbulent (f_t) flow takes place at approximately $Re = 1500$. For superfluid helium we assume that the friction mechanism at the pipe wall is the same as for normal helium. In this case, for the calculation of the Reynolds number we use the total density and velocity of the flow, but the viscosity of the normal helium component only [9].

The external heat source $\dot{q}'''_{\mathrm{ext}}$ models the heat inputs into the cooling channel, and it is usually a known, driving term. In reality, depending on the length and time scale of the external heating, it may be necessary to take into account complex heat transfer mechanisms at the wetted pipe surface that are not within the scope of this work. We finally remark that in the form above, Equations (5)–(7) are valid both in the superfluid and in the normal fluid domains, allowing continuous simulations across the phase boundary.

Boundary conditions are needed to close the problem. For compressible flow as described by the set of equations above, we know that the number and type of boundary conditions to be imposed depends on the sign of the characteristics at the boundary [10]. However, dealing with the non-linear system of equations above, we no longer have a clear guideline for the number and type of boundary conditions needed. In addition, the boundary conditions should be imposed on the Riemann invariants, rather than on the state and flow variables. The use of the Riemann invariants is not practical for our purposes and we have resorted on a more pragmatic approach that has proven to give stable results.

Helium cooling circuits are connected to manifold systems that act as large buffers at given pressure and temperature conditions, with in- and outflow at very low Mach numbers. As discussed in [2], for a flow of helium in normal state we impose pressure boundary conditions both at inflow and outflow boundaries, and temperature boundary conditions only in the case of inflow. The boundary values of pressure and temperature can be, in principle, a known function of time. In the case of superfluid helium the modification of the energy balance due to the counterflow term $\dot{q}''_{\mathrm{cf}}$ can be written alternatively as follows:

$$
\dot{q}''_{\mathrm{cf}} = -\frac{F(T,p)^{1/\eta}}{\left(\dfrac{\partial T}{\partial x}\right)^{1-1/\eta}}\frac{\partial T}{\partial x} = -\tilde{k}\frac{\partial T}{\partial x},
\tag{10}
$$

where $\tilde{k}$ is the effective conductivity, dependent on the temperature gradient. In the form above, the counterflow heat transport term resembles classical heat diffusion. The presence of this diffusion-like term in the energy equation translates into a second-order derivative term in Equation (7) for the temperature evolution. Hence, the original hyperbolic equation (for normal helium) becomes pseudo-parabolic (for superfluid helium) and we need necessarily two boundary conditions for its solution. Therefore, we have modified the boundary conditions in the case of superfluid state (i.e. for ($T \leq T_\lambda$), by imposing both pressure and temperature at inflow and outflow boundaries. In specific cases it can be useful to model symmetry boundary conditions, as in one of the test cases discussed later in the paper. This is achieved imposing zero flow and zero temperature gradient at the boundary. The same boundary condition

applies to the common case of a closed pipe inlet or outlet (e.g. a closed valve) and adiabatic conditions at the boundary.

3. FINITE ELEMENT ALGORITHM AND LINEARIZATION

The system of Equations (5)–(7) forms a non-linear system with mixed hyperbolic–parabolic character. As we have discussed in [2], no optimal technique can be defined to deal with both aspects, especially when the compressible flow is associated with thermal processes triggered by a sudden transition of a superconducting cable to the normal state. In the case of normal helium flow we have chosen a Galerkin finite element approximation in space with selective upwinding on the equations in order to damp the high-order modes associated with sound waves propagation without affecting the low-order modes associated with heat convection. The implicit time integration used permits operation at very high Courant numbers, regularly in excess of 1000, and thus does not penalize meshes with very small element sizes, necessary to improve the space resolution in regions of interest. We will discuss here only the adaptions of this basis scheme taken for the solution of the counterflow heat flux term.

We first put the system of Equations (5)–(7) in the following convenient matrix form:

$$\mathbf{m}\frac{\partial \mathbf{u}}{\partial t}+\mathbf{a}\frac{\partial \mathbf{u}}{\partial x}-\frac{\partial}{\partial x}\left(\mathbf{g}\frac{\partial \mathbf{u}}{\partial x}\right)-\mathbf{s}\mathbf{u}=\mathbf{q}, \tag{11}$$

where we have defined the vector of unknowns $\mathbf{u}$ as:

$$\mathbf{u}=\begin{bmatrix} v \\ p \\ T \end{bmatrix} \tag{12}$$

and the remaining matrices and vectors are given by:

$$\mathbf{m}=\begin{bmatrix} 1 & 0 & 0 \\ 0 & 1 & 0 \\ 0 & 0 & \rho C_v \end{bmatrix}, \tag{13}$$

$$\mathbf{a}=\begin{bmatrix} v & \dfrac{1}{\rho} & 0 \\ \rho c^2 & v & 0 \\ \rho\varphi C_v T & 0 & \rho C_v v \end{bmatrix}, \tag{14}$$

$$\mathbf{g}=\begin{bmatrix} 0 & 0 & 0 \\ 0 & 0 & \varphi\tilde{k} \\ 0 & 0 & \tilde{k} \end{bmatrix}, \tag{15}$$

$$\mathbf{s}=\begin{bmatrix} -2\dfrac{f|v|}{D_h} & 0 & 0 \\ 2\rho\varphi\dfrac{fv|v|}{D_h} & 0 & 0 \\ 2\rho\dfrac{fv|v|}{D_h} & 0 & 0 \end{bmatrix}, \tag{16}$$

$$\mathbf{q} = \begin{bmatrix} 0 \\ 0 \\ \dot{q}'''_{\text{ext}} \end{bmatrix}. \tag{17}$$

Note that in the definition of the counterflow term we have used the pseudo-diffusion form discussed previously, appearing in the diffusion matrix $\mathbf{g}$ and making explicit the second-order temperature derivative. We now discretise in space approximating the unknowns $\mathbf{u}$ with linear shape functions $\mathbf{N}$ interpolating the values at the nodes $\mathbf{U}$ of a one-dimensional mesh:

$$\mathbf{u} \approx \mathbf{N}\mathbf{U}, \tag{18}$$

and we write the system equation (11) as a weighted residual at the nodes with identical weight and shape functions. We obtain the following system of ordinary differential equations in time:

$$\mathbf{M}\frac{\partial \mathbf{U}}{\partial t} + (\mathbf{A} + \mathbf{G} - \mathbf{S})\mathbf{U} = \mathbf{Q}, \tag{19}$$

with the following definitions for the matrices $\mathbf{M}$, $\mathbf{A}$, $\mathbf{G}$, $\mathbf{S}$ and the vector $\mathbf{Q}$:

$$\mathbf{M} = \int \mathbf{N}^T \mathbf{m} \mathbf{N}\, \mathrm{d}x, \tag{20}$$

$$\mathbf{A} = \int \mathbf{N}^T \mathbf{a}\, \frac{\mathrm{d}\mathbf{N}}{\mathrm{d}x}\, \mathrm{d}x, \tag{21}$$

$$\mathbf{G} = \int \frac{\mathrm{d}\mathbf{N}^T}{\mathrm{d}x}\, \mathbf{g}\, \frac{\mathrm{d}\mathbf{N}}{\mathrm{d}x}\, \mathrm{d}x, \tag{22}$$

$$\mathbf{S} = \int \mathbf{N}^T \mathbf{s} \mathbf{N}\, \mathrm{d}x, \tag{23}$$

$$\mathbf{Q} = \int \mathbf{N}^T \mathbf{q}\, \mathrm{d}x. \tag{24}$$

So far the treatment is identical to the one exposed in Reference [2], and we refer to it for the selective upwinding procedure. In the present case, for superfluid helium, an additional matrix contribution is present in $\mathbf{G}$, namely the pseudo-diffusion term. Its approximation is given, in each finite element, by:

$$\tilde{k} \approx -\frac{F(T,p)^{1/\eta}}{\left(\dfrac{\partial N_i}{\partial x} T_i\right)^{1-1/\eta}}, \tag{25}$$

where T_i are the nodal temperatures and N_i are the nodal shape functions for node i. We can see from Equation (25) that the approximation above is potentially divergent when the gradient of temperature, at denominator, approaches zero. This situation, which corresponds physically to zero heat flux, must be dealt by a proper limiting procedure. Similarly to what was done in [12], we clamp the temperature gradient to a minimum $\gamma_{\min}$, chosen so that the corresponding counterflow heat flux (Equation (4)) is negligible. We found that values of $\gamma_{\min}$ in the range $10^{-5} \sim 10^{-6}$ K m^{-1} can be safely used without causing numerical conditioning problems for the cases presented here. Note that these values are several orders of magnitude lower than those tested in [12].

The evaluation of the matrices of Equations (20)–(24) is done analytically, taking the average value over the element for the non-linear terms appearing in the integrals. The

pseudo-diffusion term of Equation (25) is evaluated in the center of the linear, two-node elements. We finally discretize in time using the trapezoidal integration rule (superscripts indicate time stations), obtaining the following system of non-linear algebraic equations for the increments of the nodal variable $\Delta\mathbf{U}$:

$$\left[\frac{\mathbf{M}^{n+\theta}}{\Delta t}+\theta(\mathbf{A}^{n+\theta}+\mathbf{G}^{n+\theta}-\mathbf{S}^{n+\theta})\right]\Delta\mathbf{U}=(\mathbf{A}^{n+\theta}+\mathbf{G}^{n+\theta}-\mathbf{S}^{n+\theta})\mathbf{U}^{n}+\mathbf{G}^{n+\theta}, \tag{26}$$

where Δt is the time step and θ is the implicitness parameter, with typical choices of $1/2$ and 1. The system above is non-linear for any value of θ different from 0, as it implies the knowledge of the matrix coefficients at an intermediate time in the time step. The linearization procedure chosen consists of simply ignoring the non-linearity, and taking instead of Equation (26), the following linear algebraic system:

$$\left[\frac{\mathbf{M}^{n}}{\Delta t}+\theta(\mathbf{A}^{n}+\mathbf{G}^{n}-\mathbf{S}^{n})\right]\Delta\mathbf{U}=(\mathbf{A}^{n}+\mathbf{G}^{n}-\mathbf{S}^{n})\mathbf{U}^{n}+\mathbf{Q}^{n}. \tag{27}$$

The matrix on the left-hand-side is built using the results of the previous time step. The system equation (27) is finally solved at each time step by direct factorization and back-substitution.

4. ALGORITHM ANALYSIS—STABILITY AND CONVERGENCE

In the stability and accuracy analysis presented here we have concentrated on treatment of the counterflow term, using the following simplified homogenous partial differential equation:

$$C\frac{\partial U}{\partial t}-\frac{\partial}{\partial x}\left(F\frac{\partial U}{\partial x}\right)^{1/3}=0, \tag{28}$$

that can be obtained from the energy equation neglecting compressibility and source terms. Equation (28) demonstrates most of the issues without adding useless complexity to the treatment. Note that in Equation (28), we have taken for simplicity $\eta=3$, although any choice of η in the typical range of experimental data would not affect the results quoted here. Assuming constant coefficients and proceeding as outlined in the previous section, the discretization of Equation (28) on a regular mesh of spacing Δx and time step Δt becomes (subscripts indicate nodes, superscripts time stations):

$$\begin{aligned}
&\frac{C\Delta x}{6\Delta t}\left[(T_{i-1}^{n+1}+4T_{i}^{n+1}+T_{i+1}^{n+1})-(T_{i-1}^{n}+4T_{i}^{n}+T_{i+1}^{n})\right]\\
&+(1-\theta)\left[\frac{F^{1/3}}{\left(\dfrac{T_{i}^{n}-T_{i-1}^{n}}{\Delta x}\right)^{2/3}}\frac{T_{i}^{n}-T_{i-1}^{n}}{\Delta x}-\frac{F^{1/3}}{\left(\dfrac{T_{i+1}^{n}-T_{i}^{n}}{\Delta x}\right)^{2/3}}\frac{T_{i+1}^{n}-T_{i}^{n}}{\Delta x}\right]\\
&+(1-\theta)\left[\frac{F^{1/3}}{\left(\dfrac{T_{i}^{n+1}-T_{i-1}^{n+1}}{\Delta x}\right)^{2/3}}\frac{T_{i}^{n+1}-T_{i-1}^{n+1}}{\Delta x}-\frac{F^{1/3}}{\left(\dfrac{T_{i+1}^{n+1}-T_{i}^{n+1}}{\Delta x}\right)^{2/3}}\frac{T_{i+1}^{n+1}-T_{i}^{n+1}}{\Delta x}\right]=0.
\end{aligned} \tag{29}$$

We have then computed the amplification factor of the scheme above using the Von Neumann technique of Fourier decomposition of the error [16], taking into account the non-linearity

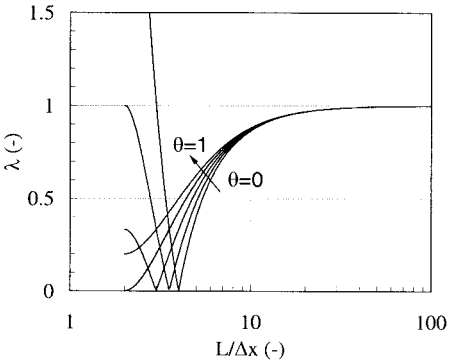

Figure 2. Amplification factor for the simplified model of transient heat transport including only the counterflow mechanism. L is the mesh length, Δx is the space step plotted for a value of $\delta = 1$. The curves plotted correspond to values of the implicitness parameters θ of 0, 1/4, 1/2, 3/4, 1. θ is monotonously increasing in the direction indicated by the arrow.

connected with the pseudo-diffusive term. The resulting amplification factor is thus non-linear:

$$\lambda = \frac{4 + 2\cos(\phi) - 6\delta(1-\theta)[(1-\cos(\phi) + i\sin(\phi))^{1/3} + (1-\cos(\phi) - i\sin(\phi))^{1/3}]}{4 + 2\cos(\phi) - 6\delta\theta[(1-\cos(\phi) + i\sin(\phi))^{1/3} + (1-\cos(\phi) - i\sin(\phi))^{1/3}]}, \quad (30)$$

where ϕ is the phase angle of the error mode considered, ranging in the interval $[0, \ldots, \pi]$, and we have introduced the parameter δ given by:

$$\delta = \frac{6\Delta t}{C\Delta x^2} \frac{F^{1/3}}{(T_i^n/\Delta x)^{2/3}}, \quad (31)$$

that resembles closely the diffusion number for a linear problem. Equation (30) cannot be handled easily to determine the stability limits corresponding to any choice of the implicitness parameter θ. Therefore, we have experimentally plotted the module of the amplification factor, and verified that, as expected, unconditional stability is obtained for $\theta \geq 1/2$ also in the non-linear case, while any choice $\theta < 1/2$ is conditionally stable (see the results plotted in Figure 2 for the case $\delta = 1$).

A second issue to address is the order of convergence of the linearized approximation of the pseudo-diffusion term (using Equation (25)). Using the equivalent differential equation of the scheme [16], and after trivial algebra, it can be shown that the linearization used in the scheme of Equation (29) based on the evaluation of the equivalent conductivity in the center of each element:

$$\frac{\partial}{\partial x}\left(F\frac{\partial T}{\partial x}\right)^{1/3} \approx \left[\frac{F^{1/3}}{\left(\dfrac{T_i - T_{i-1}}{\Delta x}\right)^{2/3}} \frac{T_i - T_{i-1}}{\Delta x} - \frac{F^{1/3}}{\left(\dfrac{T_{i+1} - T_i}{\Delta x}\right)^{2/3}} \frac{T_{i+1} - T_i}{\Delta x}\right]$$

has second-order accuracy, with an error explicitly given by:

$$\varepsilon = \frac{5}{162}\left(\frac{\partial T}{\partial x}\right)^{-8/9}\left(\frac{\partial^2 T}{\partial x^2}\right)^3 \Delta x^2 = o(\Delta x^2). \quad (32)$$

5. BENCHMARKING

Heat convection and counterflow heat transport in superfluid helium result in a highly non-linear problem that is not easily solved analytically. This is especially true because of the variation of the thermophysical properties of helium in the temperature range of interest. Hence, we have decided to validate the algorithm using available published experimental data on helium superfluid heat transport in pipes.

5.1. Steady state heat transport measurements of Srinivasan and Hoffman [17]

The first experiment chosen is from Srinivasan and Hoffman [17], who have measured steady state temperatures distribution in a pipe of length 0.8 m and 3 mm inner diameter heated over a short length in the center. Different heating power and mass flow rates were used and the temperature was recorded at eight thermometers along the pipe. Table I reports pressure, mass flow and heating power for the runs that we have chosen for the validation of the algorithm. Compared with the experiments performed, they cover the whole parameter space of the measurement set.

All simulations were performed using a uniform mesh of 200 elements over the pipe length. Convergence studies, not reported here, showed that increasing the number of elements had no effect on the solution. The steady state conditions were reached as the limit of a long transient. The initial conditions for the simulations were obtained as an approximate solution of a steady state flow with no heating. In particular, the mass flow was taken identical to the experimental values reported in Table I. The temperature distribution was assumed to be initially flat, with a value identical to the inlet temperature. The inlet pressure was taken equal to the nominal background pressure, as from Table I. The pressure drop was computed in the hypothesis of incompressible flow and constant friction factor, and the pressure distribution was assumed to be linearly decreasing from inlet to outlet. Finally, the velocity was calculated from the specified mass flow and the density, the latter dependent on the local value of temperature and pressure. Because of the small flow used in the experiments, and the short length of pipe, the pressure drop necessary to maintain the steady mass flow was negligible (10^{-3}–10^{-4} bar) as

Table I. Summary of operating conditions for the runs considered in the benchmarking against the experimental data of Srinivasan and Hoffman [17]

Pressure (Pa)	Mass flow ($g\,s^{-1}$)	Heater power (W)
2.5E5	0.329	0.169
		0.220
		0.265
		0.331
5.0E5	0.347	0.279
		0.344
		0.418
7.0E5	0.334	0.295
		0.362
		0.456
1.0E5	0.0	0.145
		0.205

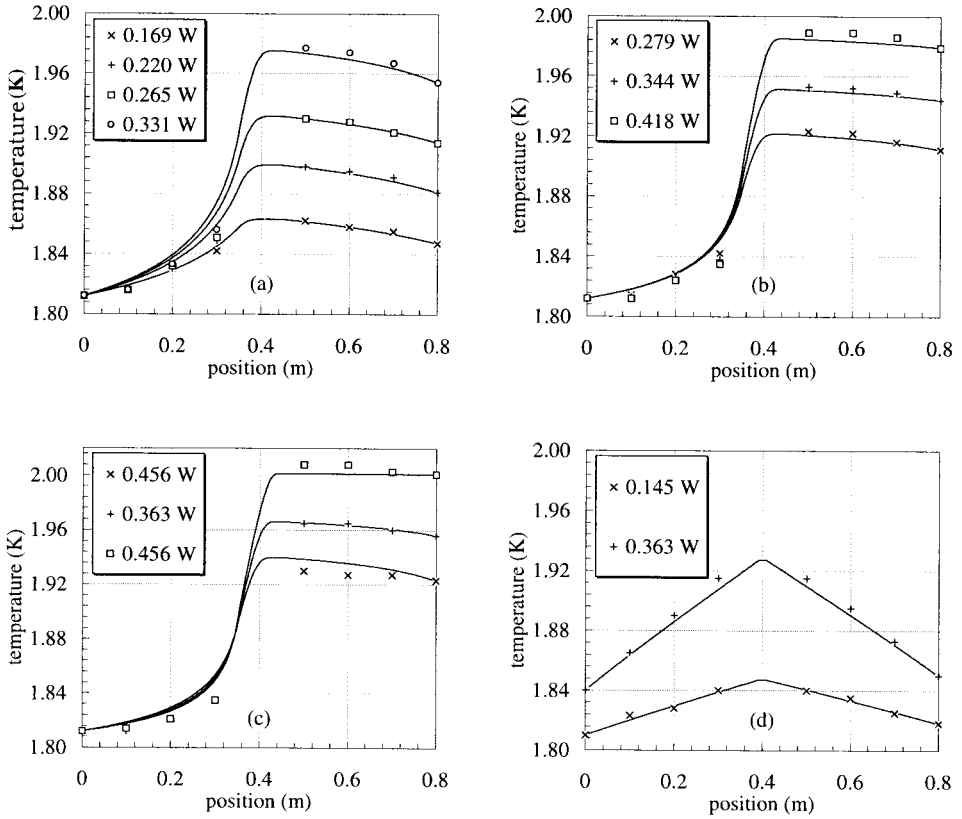

Figure 3. Comparison of experimental data from Srinivasan and Hoffman [17] with simulations. The results are grouped by operating pressure and mass flow: (a) 2.5 bar and 0.329 $g\,s^{-1}$, (b) 5 bar and 0.347 $g\,s^{-1}$, (c) 7 bar and 0.334 $g\,s^{-1}$, (d) 1 bar stagnant. Heater powers as indicated in the legends.

compared with the background pressure (1–7 bar). The initial conditions chosen were thus a good approximation of the real flow.

The simulation of the transient was then started, ramping the external heating within 5 s to the nominal steady state value of Table I. This ramp was advantageous, although not necessary, allowing large time steps (up to 1 s) to be taken from the very beginning of the transient and accelerating convergence towards steady state conditions. A 1 s time step corresponds to a Courant number of the order of 50000, that did not appear to cause instability in the solution. Inlet and outlet pressure and temperature were specified, constant in time. This is in accordance with the boundary conditions in superfluid state as detailed in Section 2. The boundary conditions for pressure were taken identical to the initial values. For temperature we used the measured values at the entry and exit sections of the pipe ($x = 0$ m and $x = 0.8$ m). Note that because of the difference that was present between the experimental values at inlet and outlet, the boundary conditions were not fully consistent with the initial temperature profile (constant temperature in space, equal to the inlet value). The temperature profile relaxed during the transient without difficulties. A total of 50–100 s of simulated time was necessary to achieve steady state conditions in all cases.

We compare temperature profiles as obtained from the experimental results (data points) and simulations (continuous lines) in Figure 3, where we have grouped the experiments by

operating pressure and mass flow. The agreement is excellent, for both forced flow (Figure 3(a)–(c)) and stagnant (Figure 3(d)) conditions, and for all heater powers.

5.2. Steady state and transient measurements of Kashani et al. [12]

The second experiment chosen is from Kashani *et al.* [12], who have measured temperatures distribution in a copper tube of 2 m length and 3 mm inner diameter, heated at its midpoint along its length. Table II reports the mass flow and heating powers for the experiments simulated. We have performed simulation using a uniform mesh of 200 elements.

Figure 4(a) shows the comparison of steady state temperature profiles as measured and simulated at an initial bath temperature of 1.95 K. To establish initial conditions and to reach the steady state we followed a procedure identical to the one presented in the previous section. The agreement between measured and simulated profiles is satisfactory.

In Figure 4(b) and (c), we report transient measurements and simulations at an initial bath temperature of 1.65 K. Figure 4(b) refers to data taken during a step heat deposition of 0.377 W, while in Figure 4(c) a rectangular heat pulse of 0.404 W was applied for a total duration of 3.5 s. In this case, we performed the full transient simulation starting from the approximate flow initial conditions. The pressure at inlet and outlet was taken constant in time. The inlet and outlet temperatures were obtained from a linear interpolation of the experimental values as a function of time. Again, the simulations compare favorably with the measurements. In transient conditions some time lag seems to appear (see Figure 4(b)), possibly due to the uncertainty on the thermophysical properties of helium in the superfluid state. Note that a lag of the same order was obtained in an independent simulations of the same experiment [14].

For these two transient cases we have reported in Figure 5(a) and (b) the velocity profiles computed at different times. Figure 5(a) refers to the step in heating power. Pressure variations during the transient with respect to the initial profile are negligible (of the order of 10^{-5} bar) for two reasons. Firstly, the characteristic time needed for the establishment of the temperature profile is much longer than the time necessary for sound waves to travel along the pipe (of the order of 20 ms at approximately 100 m s^{-1} isentropic sound speed). Secondly, the density changes associated with the transient heating are small. The mass flow is, therefore, approximately constant during the transient. The variations of velocity visible in Figure 5(a) are thus mostly associated with the small changes in the density profile under approximately constant mass flow. We note another interesting feature of superfluid helium, namely the effect of a negative expansion coefficient. A temperature increase in the superfluid state corresponds to a density increase. Therefore, in the region after the heater, where the helium is warmer, the flow *decelerates* to maintain the mass flow constant along the pipe. A similar behavior is found for the velocity profiles in the case of a rectangular heating pulse, shown in Figure 5(b). In this

Table II. Summary of conditions for the runs simulated in the benchmarking against the experimental data of Kashani e*t al.* [12]

Mass flow (g s^{-1})	Heater pulse waveform	Heater pulse duration	Heater power (W)
0.133	—	Steady state	0.123
0.215	—	Steady state	0.201
0.400	—	Steady state	0.358
0.215	Step	—	0.377
0.215	Rectangular	3.5 s	0.404

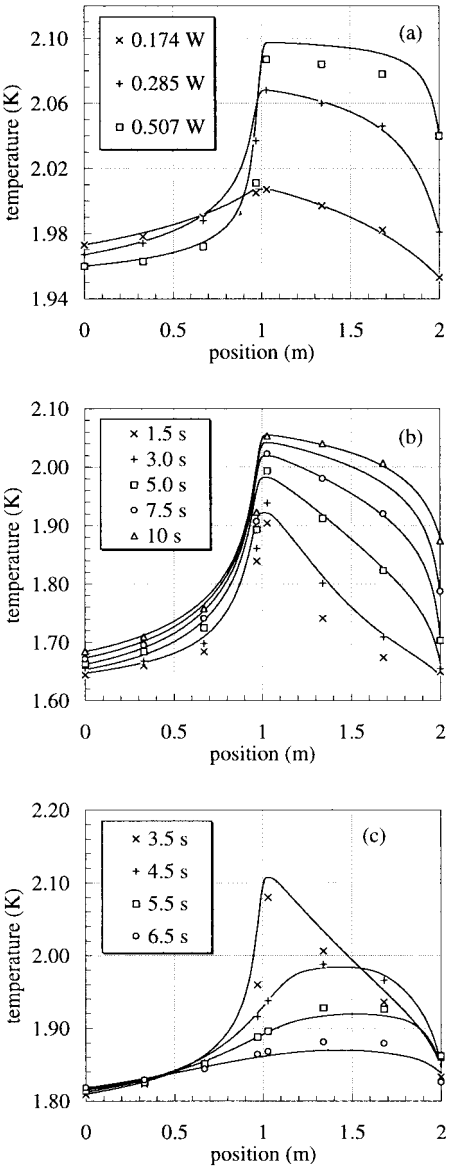

Figure 4. Comparison of experimental steady state (a) and transient heat input (b) and (c) data from Kashani *et al.* [12] with the results of simulations.

case, for long times, the velocity tends to the initial profile, as the heated helium is flushed and the temperature drops (see also Figure 4(c)). In both cases, as we already remarked, the effects are small, with typical changes in density and velocity in the range of 1–3%.

5.3. Transient measurements of Lottin and Van Sciver [18]

The last comparison has been made with the results of Lottin and Van Sciver reported from Reference [18], where a stainless steel test tube of 2.3 m length and 6 mm inner diameter was

heated within a 0.1 m section in the middle by a 0.92 J pulse lasting 0.02 s. Operating pressure was 1 bar and bath temperature 1.82 K. The simulations were performed in this case using a mesh of 800 elements, modeling only half of the pipe length and assuming symmetry conditions in the middle of the pipe. Stagnant helium at uniform temperature was taken as the initial condition. In the experiment, the test section was connected to a helium bath that acted as a heat sink of limited capacity (the temperature increased during the pulse). We have chosen to approximate this boundary condition adding a long length of pipe (1 m) to the test section and setting constant pressure and temperature, equal to the initial values, at the end of the additional pipe length. The additional length acted in the simulation as a mock-up of the buffer, allowing free evolution of the temperature at the location corresponding to end of the test section.

We report in Figure 6 the temperature increase measured at the thermometers together with the results of the simulation. Note that because of the symmetry assumption, we plot only half of the length of the test section (1.15 m). This case is particularly complex to analyze, because the energy deposited in the bath caused a local transition of state: superfluid helium is heated locally above T_λ and becomes normal helium, with much lower density and practically no heat conduction. This is correctly predicted by the simulation, which shows a localized temperature peak at early times in the center of the pipe. In the experiment, a copper tube supporting the heater wire acted as a thermal shunt along the pipe length and assisted in the recovery of the superfluid state draining heat from the normal fluid region towards the superfluid region. This

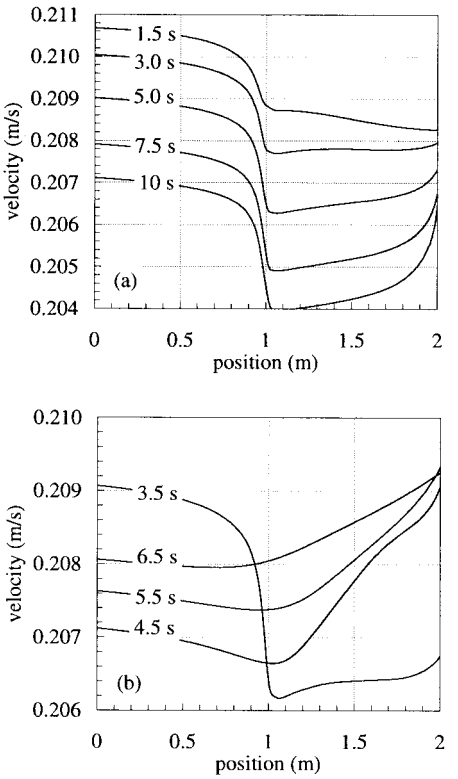

Figure 5. Calculated velocity at different times (indicated on the curves) for the transient heat input simulations of the experiments of Kashani *et al.* [12], (a) refers to a step in heating power, (b) to a rectangular heating pulse.

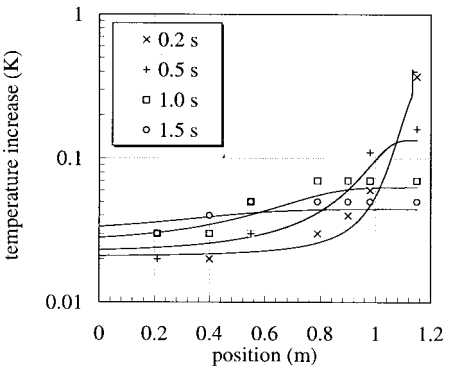

Figure 6. Comparison of simulation and experimental data on temperature increase during a heat pulse in a superfluid helium pipe as obtained by Lottin and Van Sciver [18].

particular has not been modeled in the simulation. Still we see that the simulation qualitatively predicts the spread of the temperature peak, as well as the recovery of the superfluid state, as time advances.

To demonstrate the large heat transport capability of superfluid helium we report in Figure 7 a snap-shot of the contributions to the total heat flux along the pipe, evaluated at 0.1 s. The two curves show in particular the heat flux due to the counterflow heat exchange mechanism, evaluated from the numerical solution using Equation (4), and the heat transported by mass convection, evaluated as $\rho v C_p T$. As clear from the results reported there, counterflow heat exchange is the dominating mechanism for heat transport. At 0.1 s the helium in the region between $x = 1.12$ and $x = 1.15$ m, under the heater, is in normal state. Here the counterflow heat flux is zero. Because of the symmetry condition, velocity is small in this region, and therefore convection is also negligible. Counterflow heat exchange appears as soon as the temperature is below T_λ. Close to the heater, the temperature gradient is largest, and the counterflow heat flux reaches a maximum of around 40 kW m^{-2}. Note that because of the temperature dependence of the heat conductivity function F, peaked at 1.8–1.9 K, the location of the maximum is not right at the phase transition from superfluid to normal helium, where the gradient is maximum, but slightly displaced within the superfluid region. Convection heat transfer is much smaller, of the order of 3 kW m^{-2}, and has the opposite direction to the

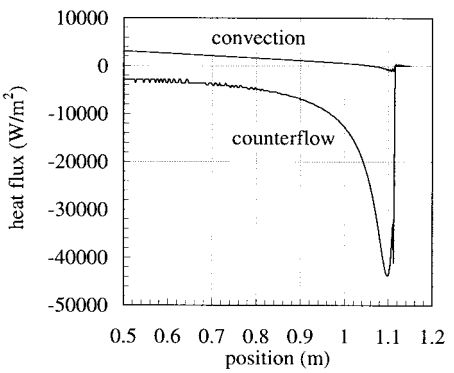

Figure 7. Heat fluxes due to the counterflow heat exchange mechanism in superfluid helium and due to convection, as computed at $t = 0.1$ s in the simulation of the experiment of Lottin and Van Sciver [18].

counterflow contribution. This is again due to the fact that the expansion coefficient is negative in superfluid helium, so that the heating induced flow is towards the heated region.

6. CONCLUSIONS

We have presented a linearized finite element algorithm for the solution of the steady state and transient one-dimensional flow of helium in superfluid state, based on an approximation of the counterflow heat exchange mechanism, and taking into account non-linear properties and compressibility phenomena. The algorithm is implicit, linearly unconditionally stable and has second-order accuracy in space. The implementation has been done as the extension of a thermohydraulic model of a superconducting cable [2], that has now augmented capability and extended validity range. The additional terms, originated by the counterflow heat exchange, did not affect the stability properties of the original algorithm for compressible flow, that can still operate at Courant number commonly in excess of 1000. Finally, we have used published experimental results to benchmark the method with satisfactory results.

APPENDIX A. NOMENCLATURE

$\mathbf{a}$, $\mathbf{A}$	matrix and discretized matrix of convention coefficients
$\mathbf{c}$	sound speed
C, C_v	specific heat and specific heat at constant volume
D_h	hydraulic diameter
f	friction factor
F	superfluid conductivity function
$\mathbf{g}$, $\mathbf{G}$	matrix and discretized matrix of diffusion coefficients
$\tilde{k}$	effective conductivity
$\mathbf{m}$, $\mathbf{M}$	matrix and discretized matrix of *mass* (time derivatives) coefficients
N, $\mathbf{N}$	nodal shape function and vector of nodal shape function
p	pressure
$\dot{q}''_{\mathrm{cf}}$	superfluid counterflow heat flux
$\dot{q}'''_{\mathrm{ext}}$	external volumetric heat flux
$\mathbf{q}$, $\mathbf{Q}$	source and discretized source vector
$\mathbf{s}$, $\mathbf{S}$	source and discretized source matrix
t	time coordinate
T, T_λ,	temperature, temperature at the lambda transition
$\mathbf{u}$, U, $\mathbf{U}$	vector of unknowns, nodal unknown and vector of nodal unknown
v, v_{s}, v_{n}	velocity, velocity of the superfluid and normal components
x	space co-ordinate

Greek letters

ε	error
δ	diffusion number
ϕ	phase angle of the error mode in the analysis of the amplification factor
$\gamma_{\min}$	minimum temperature gradient for effective conductivity evaluation
η	exponent for the temperature gradient in the counterflow heat flux
φ	Gruneisen parameter

λ	amplification factor
ν_n	viscosity of normal component
ρ, ρ_s, ρ_n,	density, density of the superfluid and normal components
θ	implicitness parameter for time integration

REFERENCES

1. S.W. Van Sciver, *Helium Cryogenics*, Clarendon Press, Oxford, 1986.
2. L. Bottura, 'A numerical model for the simulation of quench in the ITER magnets', *J. Comput. Phys.*, **125**, 26–41 (1996).
3. Y.M. Khalatnikov, *Introduction to the Theory of Superfluidity*, W.A. Benjamin, Reading, MA, 1965.
4. V. Arp, 'Heat transport through helium II', *Cryogenics*, **10**, 96–105 (1970).
5. C.J. Gorter and J.H. Mellink, 'On the irreversible processes in liquid helium II', *Physica*, **15**, 285–304 (1949).
6. S.W. Van Sciver, 'Developments in He II heat transfer and applications to superconducting magnets', *Adv. Cryo. Eng.*, **27**, 375–398 (1982).
7. T. Kitamura, K. Shiramizu, N. Fujimoto, Y.F. Rao and K. Fukuda, 'A numerical model on transient, two-dimensional flow and heat transfer in He II', *Cryogenics*, **37**, 1–9 (1997).
8. V. Arp, 'Thermodynamics of single-phase one-dimensional fluid flow', *Cryogenics*, **15**, 285–289 (1975).
9. P.L. Walstrom, J.G. Weisend II, J.R. Maddocks and S.W. Van Sciver, 'Turbulent flow pressure drop in various He II transfer system components', *Cryogenics*, **28**, 101–109 (1988).
10. L. Dresner, 'Transient heat transfer in superfluid helium–Part 11', *Adv. Cryo. Eng.*, **29**, 323–333 (1984).
11. S.W. Van Sciver, 'Heat transport in forced flow He II: analytic solution', *Adv. Cryo. Eng.*, **29**, 315–322 (1984).
12. A. Kashani, S.W. Van Sciver and J.C. Strikwerda, 'Numerical solution of forced convection heat transfer in He II', *Numer. Heat Transf.*, **16**, 213–228 (1989).
13. M.B. Gorbounov, L. Bottura, J.R. Miller and S.W. Van Sciver, 'Finite element code for quench and stability analysis of superconducting magnets cooled by He II', *Adv. Cryo. Eng.*, **41**, 335–342 (1996).
14. Y.F. Rao, Y. Inaba, T. Noda and K. Fukuda, 'Transient characteristics of He II forced flow heated at the center of a pipe line', *Cryogenics*, **36**, 219–224 (1996).
15. O.C. Zienkiewicz, *The Finite Element Method*, 4th edn., vol. II, McGraw-Hill, New York, 1991.
16. C. Hirsch, *Numerical Calculation of Internal and External Flows*, vols. I and II, Wiley, New York, 1989.
17. R. Srinivasan and A. Hoffmann, 'Investigations on cooling with forced flow of He II. Part 1', *Cryogenics*, **25**, 641–651 (1985); 'Investigations on cooling with forced flow of He II. Part 2', *Cryogenics*, **25**, 652–657 (1985).
18. J.C. Lottin and S.W. Van Sciver, 'Heat transport mechanism in a 2.3 m long cooling loop containing He II', *Proc. ICEC*, **9**, 269–272 (1982).

